ISSN 1674-1056
http://cpb.iphy.ac.cn
http://iopscience.iop.org/cpb
中国物理 B
Chinese Physics
中国物理 Chinese Physics B

Exploration of the structural and optical properties of a red-emitting phosphor K_2TiF_6: Mn^{4+}

Xi-Long Dou(豆喜龙), Xiao-Yu Kuang(邝小渝), Xin-Xin Xia(夏欣欣), Meng Ju(巨濛)

Citation: Chin. Phys. B . 2019, 28(1): 017107. **doi:** 10.1088/1674-1056/28/1/017107
Journal homepage: http://cpb.iphy.ac.cn; http://iopscience.iop.org/cpb

What follows is a list of articles you may be interested in

First-principles study on the mechanics, optical, and phonon properties of carbon chains

Jin-Ping Li(李金平), Song-He Meng(孟松鹤), Han-Tao Lu(陆汉涛), Takami Tohyama(遠山貴巳)

Chin. Phys. B . 2018, 27(11): 117101. **doi:** 10.1088/1674-1056/27/11/117101

Antiferromagnetic–ferromagnetic transition in zigzag graphene nanoribbons induced by substitutional doping

Shenyuan Yang(杨身园), Jing Li(李静), Shu-Shen Li(李树深)

Chin. Phys. B . 2018, 27(11): 117102. **doi:** 10.1088/1674-1056/27/11/117102

Effect of Mn doping on mechanical properties and electronic structure of WCoB ternary boride by first-principles calculations

Tong Zhang(张桐), Hai-Qing Yin(尹海清), Cong Zhang(张聪), Xuan-Hui Qu(曲选辉), Qing-Jun Zheng(郑清军)

Chin. Phys. B . 2018, 27(10): 107101. **doi:** 10.1088/1674-1056/27/10/107101

Electronic properties of defects in Weyl semimetal tantalum arsenide

Yan-Long Fu(付艳龙), Chang-Kai Li(李长楷), Zhao-Jun Zhang(张昭军), Hai-Bo Sang(桑海波), Wei Cheng(程伟), Feng-Shou Zhang(张丰收)

Chin. Phys. B . 2018, 27(9): 097101. **doi:** 10.1088/1674-1056/27/9/097101

Site preferences of alloying transition metal elements in Ni-based superalloy: A first-principles study

Baokun Lu(路宝坤), Chong-Yu Wang(王崇愚), Zhihui Du(都志辉)

Chin. Phys. B . 2018, 27(9): 097102. **doi:** 10.1088/1674-1056/27/9/097102

Exploration of the structural and optical properties of a red-emitting phosphor K_2TiF_6:Mn^{4+}*

Xi-Long Dou(豆喜龙)[1], Xiao-Yu Kuang(邝小渝)[1,†], Xin-Xin Xia(夏欣欣)[1], and Meng Ju(巨濛)[2,‡]

[1] *Institute of Atomic and Molecular Physics, Sichuan University, Chengdu* 610065, *China*
[2] *School of Physical Science and Technology, Southwest University, Chongqing* 400715, *China*

(Received 10 October 2018; revised manuscript received 20 November 2018; published online 25 December 2018)

The exploration of the appropriate red phosphor with good luminescence properties is an important issue in the development of current white light-emitting diode (WLED) devices. Transition metal Mn-doped compounds are fascinating luminescent materials. Herein, we performed a systematic theoretical study of the microstructure and optical properties of K_2TiF_6:Mn^{4+} using the CALYPSO structure search method in combination with first-principles calculations. We uncovered a novel structure of K_2TiF_6:Mn^{4+} with space group P-3m1 symmetry, where the impurity Mn^{4+} ions are accurately located at the center of the MnF_6 octahedra. Based on our developed complete energy matrix diagonalization (CEMD) method, we calculated transition lines for $^2E_g \rightarrow {}^4A_2$, $^4A_2 \rightarrow {}^4T_2$, and $^4A_2 \rightarrow {}^4T_2$ at 642 nm, 471 nm, and 352 nm, respectively, which are in good agreement with the available experimental data. More remarkably, we also found another transition ($^4A_2 \rightarrow {}^2T_2$) that lies at 380 nm, which should be a promising candidate for laser action.

Keywords: crystal structures, first-principles calculations, K_2TiF_6

PACS: 71.15.Mb, 71.20.–b, 61.50.–f **DOI:** 10.1088/1674-1056/28/1/017107

1. Introduction

Since their discovery in the 1990s, white light-emitting diodes (WLEDs) have received widespread attention because of their unique advantages, such as low loss, long lifetime, high efficiency, low environmental harm, and high thermal stability.[1–8] However, WLEDs fabricated by the yellow phosphor YAG:Ce and a blue InGaN chip[9,10] have a poor color rendering index (< 80) and a high correlated color temperature (> 6000 K) due to the lack of red emission components in their spectra,[11–13] which severely limits their application. To solve this problem, a significant amount of effort has been made to develop red-emitting materials. Interestingly, $M_2Si_5N_8$:Eu^{2+} (M = Ca, Sr, and Ba) and $CaSiAlN_3$:Eu^{2+} can make up for defects in the color rendering index and color temperature, but the serious reabsorption between nitride phosphors and YAG:Ce^{3+} reduces the luminous efficiency of these WLEDs.[14,15] In addition, their broadband emissions are over 650 nm, beyond the applicable bounds of human eyes.[16] It is therefore necessary to explore a new red luminescent material for WLEDs.

Mn^{4+}-doped fluorides have the characteristics of low phonon energy and high stability and thus are highly suitable red-emitting phosphors for use in WLEDs. In comparison with rare earth ions, the transition metal Mn^{4+} ion has a $3d^3$ valence electronic configuration and is extremely sensitive to different lattice environments. Many researchers have made great effort to investigate various Mn^{4+}-activated fluoride phosphors, such as AXF_6:Mn^{4+} (A = K, Na, Rb, Cs, NH_4, Ba, Zn and X = Si, Ge, Zr, Ti, Sn). Interestingly, Mn^{4+}-doped K_2TiF_6 was evaluated to be an excellent candidate because of its many unique advantages, particularly its higher thermal stability and fine color stability, which make this material very popular.[17–28] Experimental results suggested that K_2TiF_6 has a hexagonal crystal structure in space group P-3m1.[29] The Ti^{4+} ion is located at the center of six nearest-neighbor F ions and forms an octahedral structure, and the K^+ ion combines with the nearest-neighbor F ions to form a polyhedral structure. Mn^{4+} in Mn^{4+}-doped K_2TiF_6 prefers substitution of the Ti^{4+} ion and is coordinated with six F^- ions to form an octahedral structure. The high positive charge of the Mn^{4+} ion easily causes a strong crystal field, which can lead to energy-level splitting when Mn^{4+} is located at the geometric center of K_2TiF_6. Experimental results revealed that emission lines located at approximately 630 nm should be attributed to the spin-forbidden transition $^2E_g \rightarrow {}^4A_2$. Another two broadband absorption peaks are located at approximately 360 nm and 460 nm, corresponding to the spin-allowed transitions $^4A_2 \rightarrow {}^4T_1$ and $^4A_2 \rightarrow {}^4T_2$, which match well with the other components of WLEDs. Furthermore, the loss of the spectrum at 550 nm effectively avoids reabsorption and improves the efficiency of WLEDs. To date, many research groups have successfully synthesized the red K_2TiF_6:Mn^{4+} phosphor using different methods, such as wet chemical etching, co-

*Project supported by the National Natural Science Foundation of China (Grant No. 11574220), Fundamental Research Funds for the Central Universities, China (Grant No. SWU118055), and the Special Program for Applied Research on Super Computation of the NSFC-Guangdong Joint Fund (the second phase), China.
†Corresponding author. E-mail: scu_kuang@163.com
‡Corresponding author. E-mail: mengju@swu.edu.cn
© 2019 Chinese Physical Society and IOP Publishing Ltd

precipitation, and cation exchange procedures.[30–32] Excitingly, the photoluminescence quantum efficiency can reach as high as 98% through cation exchange synthesis. Liao *et al.*[30] investigated the properties of the K_2TiF_6:Mn^{4+} phosphor by x-ray diffraction, scanning electron microscopy, Raman spectroscopy, decay curve analysis, Fourier transform infrared spectroscopy, and photoluminescence. Bicanic *et al.*[33] devised a model phosphor mixture composed of YAG:Ce and K_2TiF_6:Mn^{4+} by the color-corrected analysis of multiple phosphors (CCAMP), which improved warm white light emission at powers up to 5 kW/cm^2. Zhou *et al.*[34] successfully developed a waterproof, narrow-band fluoride phosphor, K_2TiF_6:Mn^{4+}, through a facile superhydrophobic surface-modification strategy (i.e., using superhydrophobic surface modification with octadecyltrimethoxysilane on K_2TiF_6 surfaces), making WLEDs more accessible. However, to the best of our knowledge, there are no theoretical studies on the local structure, location site, or electronic structure of Mn^{4+}-doped K_2TiF_6, and absorption spectra have not been reported either experimentally or theoretically.

Density functional theory (DFT) is one of the most popular approximation methods in computational physics and materials research and has been widely used to address such problems.[35–40] In particular, strong on-site Coulomb repulsion (U) is introduced based on first principles, which greatly improves the reliability of the calculation result of systems with strong electronic correlations.[41–44] In this work, we first obtained ground-state structures, addressed the location site, and explored the electronic structure of Mn^{4+}-doped K_2TiF_6 using the CALYPSO (crystal structure analysis by particle swarm optimization)[45–49] structural prediction method combined with first-principles calculations. Next, we calculated the optical absorption of the octahedral Mn^{4+} center in K_2TiF_6 by diagonalizing the complete energy matrices for a $3d^3$ ion configuration in a trigonal ligand field. Simultaneously, to confirm the correctness of our method and provide a reliable method for other transition metal-doped systems, we used the same method to study the spectrum of Mn^{4+} in Cs_2TiF_6 systems.

2. Computational methods

Extensive structural searches of K_2TiF_6:Mn^{4+} under 1 atm are performed using the CALYPSO structure prediction method. This method has been demonstrated to be efficient for a variety of systems, ranging from elements to binary and ternary compounds.[50–53] The variable-cell approach is used with up to 108 atoms. The top 30 structures with relatively low energy are reoptimized in the structure searches. The structural relaxation and electronic property calculations are performed using the Perdew–Burke–Ernzerhof (PBE) functional within the generalized gradient approximation (GGA) as implemented in theVienna *ab-initio* simulation package (VASP) code.[54,55] The frozen-core all-electron projector-augmented wave (PAW) method is applied to $3s^23p^64s$, $3s^23p^63d^24s^2$, $1s^22s^22p^5$, and $3s^23p^63d^54s^2$, which are the valence electrons for K, Ti, F, and Mn, respectively. A cut-off energy of 500 eV is chosen for the total energy calculations of all structures, which is sufficient for the electron wavefunction extending to the plane-wave functions. A $3\times3\times2$ Monkhorst–Pack k mesh is used as the integration space over the Brillouin zone to ensure that the total energy is well converged to less than 1 meV/atom. To further adjust the 3d electron configuration contribution of Mn^{4+}, the DFT+U method is employed to handle the strong exchange correlation function of electrons, and the value of U added on the Mn 3d orbital is 4.0 eV.[56,57]

Mn^{4+} belongs to the $3d^3$ electronic configuration, with the high-spin ground-state spectral term $^4A_2$ ($S=3/2$). In the absence of a magnetic field, the interaction Hamiltonian in the crystal field for a $3d^3$ ion configuration can be expressed as[58]

$$\begin{aligned}\hat{H} &= \hat{H}_0+\hat{H}_{ee}+\hat{H}_{SO}+\hat{H}_{CF}\\ &= \hat{H}_0+\sum_{i<j}e^2\Big/r_{i,j}+\sum_{i=1}^{n}\zeta l_i s_i+\sum_{i=1}^{n}V_i,\end{aligned}\tag{1}$$

where $\hat{H}_0$ represents the contribution of spherical symmetric partial interactions, $\hat{H}_{ee}$ is the interaction between electrons, $\hat{H}_{SO}$ is the interaction of the electron spin–orbit coupling, and $\hat{H}_{CF}$ is the interaction between electrons and ligands. The ligand field potential (V_i) and ligand field parameter are described in the supporting information. Utilizing the $|J,M_J\rangle$ basis functions, the 120×120 energy matrix is derived according to the perturbation Hamiltonian (1) for the $3d^3$ ion configuration, where the matrix elements are the functions of the Racah parameters B and C and the spin–orbit coupling coefficient ζ.

3. Results and discussion

3.1. Structure and electronic properties

The space group of K_2TiF_6 is P-3m1, its unit cell contains two potassium atoms, one titanium atom, and six fluorine atoms. We first performed the ground-state structure prediction of K_2TiF_6 by CALYPSO using the chemical composition K : Ti : F = 2 : 1 : 6 as the input information under ambient pressure conditions and found the K_2TiF_6 structure to be in space group P-3m1, which is in accordance with the experimental results. This fact further confirms the reliability of the prediction method. Next, we reoptimized the structure of K_2TiF_6 using the local density approximation (LDA) and generalized gradient approximation (GGA) within the VASP code for the lowest energy structure. The calculated results are listed in Table S1 (supporting information), which shows that the GGA is a more accurate method for optimizing the

structure of K_2TiF_6 than the LDA. To further explore the structure of Mn^{4+}-doped K_2TiF_6 at the nominal concentration,[59] we searched the evolutionary variable-cell structure prediction structure up to 108 atoms with the input chemical composition ratio of Mn : K : Ti : F = 1 : 24 : 11 : 72 at ambient pressure. The lowest energy structures of pure K_2TiF_6 and Mn^{4+}-doped K_2TiF_6 are displayed in Fig. 1. Figure 1 shows that the Mn^{4+} ion will be more inclined to replace the vertex Ti atom and locate on Wyckoff 1*a* (0.0, 0.0, 0.0) and, along with six F^- ions, will form a regular octahedral $[MnF_6]^{2-}$ cluster in the D_{3d} point symmetry group. There is no apparent distortion compared to the octahedral $[TiF_6]^{2-}$ cluster structure, and their bond lengths and bond angles are very close, which may be attributed to the similar radius and identical valence state of the Ti^{4+} (0.605 Å) and Mn^{4+} (0.53 Å) ions. At the same time, in Fig. S1, we give another structure of Mn^{4+}-doped K_2TiF_6 whose energy is very close to the ground-state one. From Fig. S1, we find that Mn substituted Ti at different sites and located on Wyckoff 1*b* $(0.0, -1.0, 0.5)$, with the same space group (*P*-3*m*1) as the one in Fig. 1. The lattice constants, unit cell volumes, and corresponding relative energies are listed in Table S2, which indicate that the two structures are very similar. Thus, this structural information and the lowest energy structure have equally important theoretical significance for understanding the experimental observations, as well as mining the application potential of the Mn-doped K_2TiF_6 system. As an effective means of structural analysis, the XRD patterns of pure and doped K_2TiF_6 were calculated to further identify the accuracy of the predicted structures by comparing these spectra to the experimental results. As displayed in Fig. 2, the peaks and intensities of the spectra for (a) K_2TiF_6 and (b) Mn-doped K_2TiF_6 are in good agreement with the experimental data in the 2θ range of 15° to 50°,[59] which indicates that our predicted structures are reasonable. To determine the thermodynamic stability of Mn^{4+} in the K_2TiF_6 system, the formation energies (E_f) are computed by the following equation:[60]

$$E_f = E_1 + E_0 - m\mu_m + n\mu_n, \tag{2}$$

where E_1 and E_0 are the total energies of the system with and without Mn^{4+}, respectively; m and n are the numbers of dopant (Mn) atoms and substituted (Ti) atoms in the host lattice, respectively; and μ_m and μ_n are the chemical potentials for Mn and Ti atoms, respectively. We chose stable bulk MnF_4 and TiF_4 as references to evaluate the chemical potentials of the Mn and Ti atoms; for F atoms, μ_f is half the chemical potential of gas-phase F_2. The calculated formation energy is −1.5442 eV, which indicates that Mn atoms substitute vertex Ti atoms and that K_2TiF_6 is able to form a stable structure with exothermic energy.

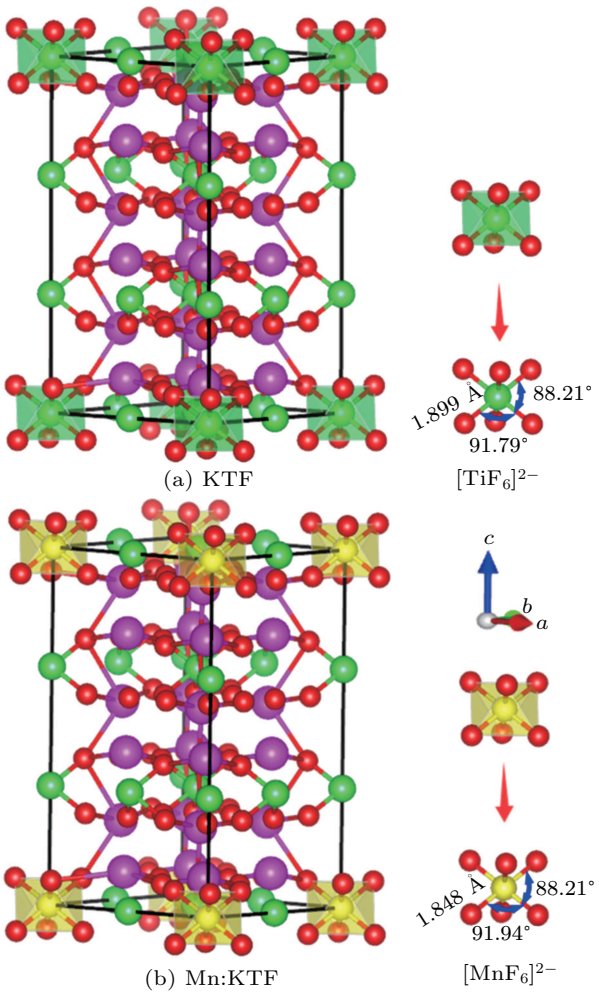


Fig. 1. Coordination structures of optimized (a) K_2TiF_6 (KTF) and (b) Mn^{4+} doped KTF. The pink, green, red, and yellow spheres represent K, Ti, F, and Mn, respectively.

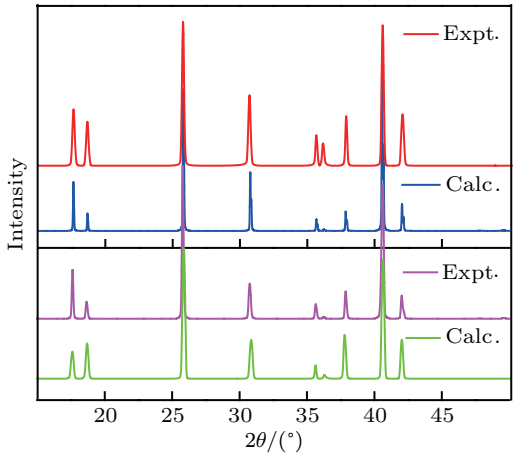


Fig. 2. Comparison of the simulated XRD patterns with experimental data for (a) K_2TiF_6 and (b) K_2TiF_6:Mn crystals.

Figure 2 shows the energy-band structure and the total and partial density of states (DOS) for pure and Mn-doped K_2TiF_6 along the high-symmetry direction of the Brillouin zone, including the spin–orbit effect. It should be noted that all the values are subtracted by the Fermi energy, and the zero-point energy is equivalent to the Fermi level. K_2TiF_6 is an

insulator with a direct gap of 4.33 eV, which is close to the value (4.73 eV) calculated by Jain *et al.*[61] In terms of the calculated band gap, the true band gap is estimated to be approximately 7–8 eV. To provide a better description of the d states of Mn^{4+} and obtain an appropriate band structure, we used the GGA+U approach to examine the Mn-doped K_2TiF_6 system, choosing $U_{eff} = 4.0$ eV. This method has been successfully applied to the study of transition element-doped systems.[62] The results show that the band gap is reduced to 2.12 eV for Mn-doped K_2TiF_6. The small band gap suggests that Mn^{4+} can effectively improve electron transport from the valence band to the conduction band when doped into K_2TiF_6 systems, leading to a shift from an insulator to a semiconductor. The formation of these gaps and the origin of all calculated bands can be well interpreted and extended by means of the DOS diagram. Figure 3 shows that the conduction band and valence band are mainly composed of p and d states. Most notably, unlike pure K_2TiF_6, the hybridization between the d state of Mn and the p state of F leads to some additional peaks in the DOS diagram of Mn-doped K_2TiF_6, which decreases the total energy and has a great influence on the emission energy.[63] We hope that our current theoretical results can provide useful guidance for further experimental investigations.

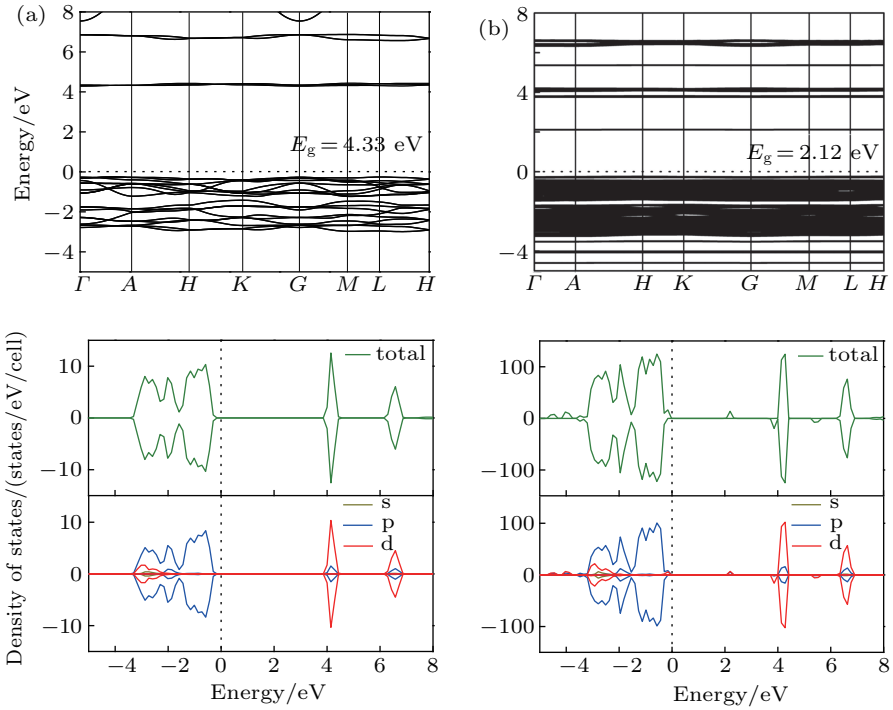


Fig. 3. Calculated band structures and total and partial DOS of (a) K_2TiF_6 and (b) K_2TiF_6:Mn. The dotted line represents the Fermi level.

3.2. Spectra properties

The Mn^{4+} ion has a $3d^3$ configuration, which possesses five-fold degenerate d orbitals and splits into two-fold and three-fold degenerate e_g and t_{2g} states due to the octahedral field, as shown in Figs. 4(a) and 4(b). The energy gap between the t_{2g} and e_g levels is $10D_q$, where D_q is the crystal field parameter. There are 120 possible scenarios for electronic placement, and the interaction of electrons in the $3d^3$ configuration may induce eight spectral terms (namely, ^4F, ^4P, ^2P, $^2D_{1,2}$, ^2F, ^2G, and ^2H, where the ^4F term represents the ground state). The effect of a crystal field splits the ^4F term further into $^4A_2$, $^4T_1$, and $^4T_2$ levels, and the ^2G term splits into ^2E, $^2T_1$, and $^2T_2$ levels. To determine the transition energy, we construct a 120×120 energy matrix for a $3d^3$ ion configuration, employing the $|J,M_J\rangle$ basis functions. The matrix elements are the functions of the Racah parameters B and C, the spin–orbit coupling coefficient ζ, and the ligand field parameters B_{20}, B_{40}, B^c_{43}, and B^s_{43}. B and C are mainly dependent on the repulsive energy between the individual d electrons, and the values of the Racah parameters B and C are 605 and 4061, which was reported by Zhu *et al.*[32] The spin–orbit coupling coefficient can be expressed as $\zeta = N^2\zeta_0$ to reduce the adjustable factor in relation to the covalence reduction effect, where N is the covalence reduction factor, which can be obtained from the approximate formula $N^2 = (\sqrt{B/B_0} + \sqrt{C/C_0})/2$,[64] and B_0, C_0, and ζ_0 represent the free Mn^{4+} ion parameters, whose values are $B_0 = 1160$, $C_0 = 4303$, and $\zeta_0 = 405$.[65] Because $[MnF_6]^{2-}$ belongs to the D_{3d} point group, the ligand field parameter B^s_{43} term is zero, and the other ligand field parameters are described in the supporting information. We introduce two parameters R and θ to describe the Mn–O bond length and the angle between the Mn–O bond and the C_3 axis, which are 1.8478 Å and 56.12°, respectively, in Fig. 1. A_4 (see the Supporting Information) is

almost constant and can be determined from the optical spectrum and the Mn–F bond length. Thus, $A_4 = 30.06$ a.u. and $A_2 = 12.41$ a.u. were estimated and used in our calculation. The optical spectra of the Mn^{4+}-doped K_2TiF_6 crystal were calculated via diagonalized complete matrices, and the results are shown in Table 1. According to the Tanabe–Sugano energy diagram and configurational coordinate[66,67] model of Mn^{4+} in octahedral coordination shown in Figs. 4(c) and 4(d), the absorption peaks located at 471 nm and 352 nm are assigned to the spin-allowed transitions $^4A_2 \rightarrow {}^4T_2$ and $^4A_2 \rightarrow {}^4T_1$. The emission peak at 642 nm is derived from the spin-forbidden transition $^2E_g \rightarrow {}^4A_2$, which is not susceptible to the crystal field strength, such that the energy of the emission peak will not change too drastically with the crystal field strength, as shown in Table S3. Our results are consistent with the experimental results.[32,59,68] The $^4A_2 \rightarrow {}^2T_1$ transition is located at 578 nm, which is in good agreement with the result reported by Zhu *et al.*[32] The $^4A_2 \rightarrow {}^2T_2$ transition lies at 380 nm, which is distributed between the ultraviolet and visible regions and was first reported by us. To further verify the reliability of our calculation method, we calculated the spectrum of Cs_2TiF_6. Cs_2TiF_6 is an analog of K_2TiF_6 in the same space group.[69] Experiments have shown that Mn substitutes Ti in the Cs_2TiF_6 system, forming octahedral $[MnF_6]^{2-}$ clusters with D_{3d} symmetry. We obtained its structure using the atomic substitution method and list the structure and its structural parameters in Fig. S2 and Table S4, respectively. The Racah parameters are $B = 657$ and $C = 3695$, which were reported by Hasan and Manson.[70] Our calculation results are in good agreement with the experimental data reported by Zhou *et al.*[71] shown in Table 1. In addition, we first identified two other absorption lines located at 603 nm and 408 nm, corresponding to the $^4A_2 \rightarrow {}^2T_1$ and $^4A_2 \rightarrow {}^2T_2$ transitions, respectively. These findings will be of great significance for guiding future experiments and developing applications of laser materials.

Table 1. The calculated and observed optical absorption spectra for Mn^{4+} ions in K_2TiF_6. All values are in units of nm.

		^2E_g	$^2T_1$	$^4T_2$	$^2T_2$	$^4T_1$
K_2TiF_6	Observed[32]	630	580	471	–	348
	Observed[59]	633	–	460	–	360
	Observed[68]	632	–	465	–	350
	Calculated	642	578	471	380	352
Cs_2TiF_6	Observed[71]	632	–	474	–	363
	Calculated	621	603	474	408	357

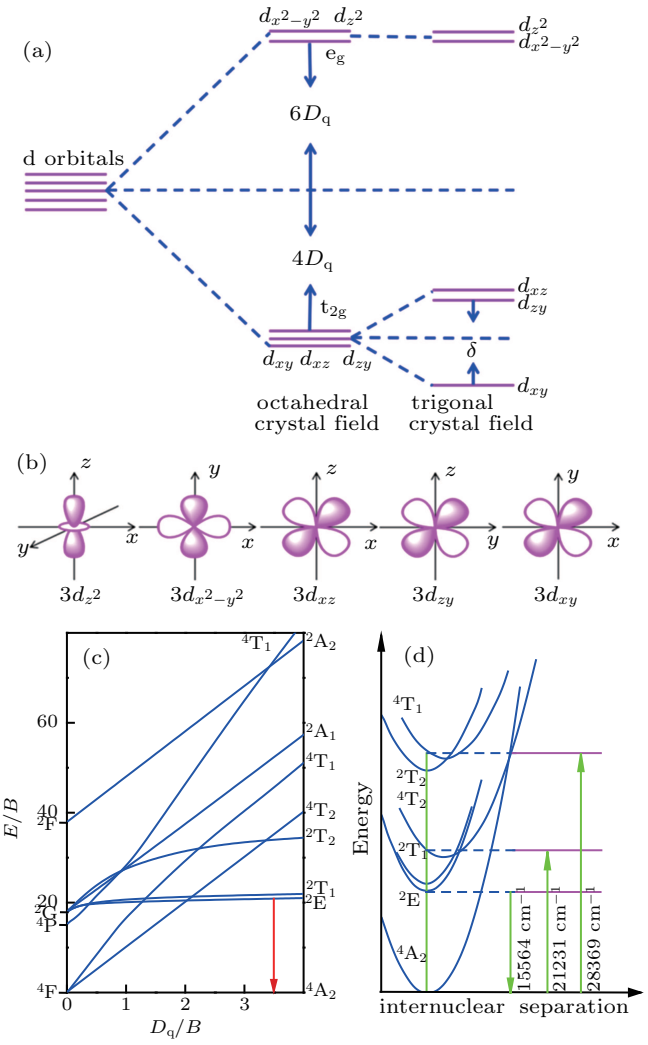


Fig. 4. (a) Energy level splitting of d^3 configuration in octahedron field. (b) Atomic orbital angle distribution diagram of d. (c) Tanabe–Sugano diagram for the d^3 electron configuration in the octahedral crystal field. (d) Configurational coordinate diagram for Mn^{4+} in K_2TiF_6.

4. Conclusions

We performed a comprehensive study of K_2TiF_6:Mn^{4+} using the CALYPSO structural search method and first-principles calculations. We identified the P-3m1 structure of Mn^{4+}-doped K_2TiF_6 under atmospheric pressure, which shows that the Mn ion substitutes the vertex Ti ion and then forms an octahedron with local D_{3d} symmetry. The accurate energy-band and DOS calculations indicate that the doped Mn ion reduces the band gap of K_2TiF_6 to 2.12 eV, which leads to an insulator-to-semiconductor transition in K_2TiF_6:Mn^{4+}. We calculated the optical absorption spectrum of K_2TiF_6:Mn^{4+} using the CEMD method. The calculated transition lines are in good agreement with the available experimental data. Furthermore, we found another promising transition line ($^4A_2 \rightarrow {}^2T_2$) located at 380 nm, which enriches the energy transition of K_2TiF_6:Mn^{4+}. We expect this new transition to be experimentally identified in the near future.

Acknowledgment

Parts of the calculations were performed using the Cherry Creek Supercomputer of the UNLV's National Supercomputing Institute.

References

[1] Ki W and Li J 2008 *J. Am. Chem. Soc.* **130** 8114
[2] Schubert E F and Kim J K 2005 *Science* **308** 1274
[3] Pimputkar S, Speck J S, DenBaars S P and Nakamura S 2009 *Nat. Photon.* **3** 180
[4] Bai X, Caputo G, Hao Z, Freitas V T, Zhang J, Longo R L, Malta O L, Ferreira R A S and Pinna N 2014 *Nat. Commun.* **5** 5702
[5] Wang L, Zhang H, Wang X J, Dierre B, Suehiro T, Takeda T, Hirosaki N and Xie R J 2015 *Phys. Chem. Chem. Phys.* **17** 15797
[6] Pust P, Weiler V, Hecht C, Tücks A, Wochnik A S, Henß A K, Wiechert D, Scheu C, Schmidt P J and Schnick W 2014 *Nat. Mater.* **13** 891
[7] Huang X 2014 *Nat. Photon.* **8** 748
[8] Oh J H, Eo Y J, Yoon H C, Huh Y D and Do Y R 2016 *J. Mater. Chem. C.* **4** 8326
[9] Schlotter P, Baur J, Hielscher C, Kunzer M, Obloh H, Schmidt R and Schneider J 1999 *Mater. Sci. Eng. B* **59** 390
[10] Daicho H, Iwasaki T, Enomoto K, Sasaki Y, Maeno Y, Shinomiya Y, Aoyagi S, Nishibori E, Sakata M, Sawa H and Matsuishi S 2012 *Nat. Commun.* **3** 1132
[11] Xie R J and Hirosaki N 2007 *Sci. Technol. Adv. Mat.* **8** 588
[12] Jang H S, Im W B, Lee D C, Jeon D Y and Kim S S 2007 *J. Lumin.* **126** 371
[13] Zhang R, Lin H, Yu Y, Chen D, Xu J and Wang Y 2014 *Laser Photon. Rev.* **8** 158
[14] Sakuma K, Omichi K, Kimura N, Ohashi M, Tanaka D, Hirosaki N, Yamamoyo Y, Xie R J and Suehiro T 2004 *Opt. Lett.* **29** 2001
[15] Piquette A P, Hannah M E and Mishra K C 2012 *ECS Trans.* **41** 1
[16] Piao X, Machida K I, Horikawa T, Hanzawa H, Shimomura Y and Kijima N 2007 *Chem. Mater.* **19** 4592
[17] Wang T, Gao Y, Chen Z, Huang Q, Wu L, Huang Y, Liao S and Zhang H 2017 *J. Lumin.* **188** 307
[18] Wang Z, Zhou Y, Yang Z, Liu Y, Yang H, Tan H, Zhang Q and Zhou Q 2015 *Opt. Mater.* **49** 235
[19] Lin C C, Meijerink A and Liu R S 2016 *J. Phys. Chem. Lett.* **7** 495
[20] Xu Y K and Adachi S 2011 *J. Electrochem. Soc.* **158** J58–J65
[21] Lv L, Chen Z, Liu G, Huang S and Pan Y 2015 *J. Mater. Chem. C* **3** 1935
[22] Wang T, Gao Y, Chen Z, Huang Q, Song B, Huang Y, liao S and Zhang H 2017 *J. Mater. Sci-Mater. El.* **28** 11878
[23] Tang F, Su Z, Ye H, Wang M, Lan X, Phillips D L, Cao Y and Xu S 2016 *J. Mater. Chem. C* **4** 9561
[24] Han T, Lang T, Wang J, Tu M and Peng L 2015 *RSC Adv.* **5** 100054
[25] Fang M H, Wu W L, Jin Y, Lesniewski T, Mahlik S, Grinberg M, Brik M G, Srivastava A M, Chiang C Y, Zhou W and Jeong D 2018 *Angew. Chem. Int. Edit.* **57** 1797
[26] Lian H, Huang Q, Chen Y, Li K, Liang S, Shang M, Liu M and Lin J 2017 *Inorg. Chem.* **56** 11900
[27] Nguyen H D and Liu R S 2016 *J. Mater. Chem. C* **4** 10759
[28] Wei L L, Lin C C, Fang M H, Brik M G, Hu S F, Jiao H and Liu R S 2015 *J. Mater. Chem. C* **3** 1655
[29] Bel O 2000 *Acta Crystallogr. C* **56** 521
[30] Liao J, Nie L Zhong L Gu Q and Wang Q 2016 *Luminescence* **31** 802
[31] Liao C, Cao R, Ma Z, Li Y and Dong G 2013 *J. Am. Ceram. Soc.* **96** 3552
[32] Zhu H, Lin C C, Luo W, Shu S, Liu Z, Liu Y, Kong J, Ma E, Cao Y R, Liu S and Chen X 2014 *Nat. Commun.* **5** 4312
[33] Bicanic K T, Li X, Sabatini R P, Hossain N, Wang C F, Fan F, Liang H, Hoogl and S 2016 *ACS Photon.* **3** 2243
[34] Zhou Y Y, Song E H, Deng T T and Zhang Q Y 2017 *ACS Appl. Mater. Inter.* **10** 880
[35] Sun J P, Zhang D and chang K 2017 *Chin. Phys. Lett.* **34** 027102
[36] Dai X, Le C C, Wu X X, Qin S S, Lin Z P and Hu J P 2016 *Chin. Phys. Lett.* **33** 127301
[37] Hu Y J, Xu S L, Wang H, Liu H, Xu X C and Cai Y X 2016 *Chin. Phys. Lett.* **33** 106102
[38] Murtaza G, Khan A A, Yaseen M, Laref A, Ullah N and ur Rahman I 2018 *Chin. Phys. B* **27** 047102
[39] Benlamari S, Bendjeddou H, Boulechfar R, Korba S A, Meradji H, Ahmed R and Omran S B 2018 *Chin. Phys. B* **27** 037104
[40] Yue Y, Song Y and Zuo X 2018 *Chin. Phys. B* **27** 037102
[41] Liu P, Wang W H, Wang W C, Cheng Y H, Lu F and Liu H 2017 *Chin. Phys. Lett.* **34** 027101
[42] Stashans A and Rivera K 2016 *Chin. Phys. Lett.* **33** 097102
[43] Mahmood Q, Yaseen M, Bhamu K C, Mahmood A, Javed Y and Ramay S M 2018 *Chin. Phys. B* **27** 037103
[44] Ahmed N, Mukhtar S, Gao W and Ilyas S Z 2018 *Chin. Phys. B* **27** 033101
[45] Zhu L, Liu H, Pickard C J, Zou G and Ma Y 2014 *Nat. Chem.* **6** 644
[46] Lu S, Wang Y, Liu H, Miao M S and Ma Y 2014 *Nat. Commun.* **5** 3666
[47] Wang Y, Miao M, Lv J, Zhu L, Yin K, Liu H and Ma Y 2012 *J. Chem. Phys.* **137** 224108
[48] Wang Y, Lv J, Zhu L and Ma Y 2012 *Comput. Phys. Commun.* **183** 2063
[49] Wang Y, Lv J, Zhu L and Ma Y 2010 *Phys. Rev. B* **82** 094116
[50] Lu C, Li Q, Ma Y and Chen C 2017 *Phys. Rew. Lett.* **119** 115503
[51] Lu C and Chen C 2018 *J. Phys. Chem. Lett.* **9** 2181
[52] Cheng L, Shuai Z, Yu Z, Da-Wei Z Z, Chao-Zheng H and Zhi-Wen L 2014 *J. Alloy. Compd.* **597** 119
[53] Lu C, Amsler M and Chen C 2018 *Phys. Rev. B* **98** 054102
[54] Jin Y, Fang M H, Grinberg M, Mahlik S, Lesniewski T, Brik M G, Lou G Y, Lin J G and Liu R S 2016 *Acs. Appl. Mater. Inter.* **8** 11194
[55] Brik M G 2010 *Solid State Commun.* **150** 1529
[56] Nava-Avendaño J, Dompablo M E, Frontera C, Ayllón J A and Palacín M R 2015 *Solid State Ionics* **278** 106
[57] Jain A, Hautier G, Moore C J, Ong S P, Fischer C C, Mueller T, Persson K A and Ceder G A 2011 *Comput. Mater. Sci.* **50** 2295
[58] Mao A J, Kuang X Y, Wan H and Huang X F 2008 *J. Alloys Compd.* **448** 6
[59] Du M, Tang F, Long J, Ma C, Yuan X, Zhang J, Wen Z, Ma R and Cao Y 2016 *Mater. Res. Bull.* **83** 316
[60] Lim J M, Kim D, Lim Y G, Park M S, Kim Y J, Cho M and Cho K 2015 *J. Mater. Chem. A* **3** 7066
[61] Jain A, Ong S P, Hautier G, Chen W, Richards W D, Dacek S, Cholia S, Cunter D Skinner D, Ceder C and Persson K A 2013 *APL Mater.* **1** 011002
[62] Yang K, Li D F, Huang W Q, Xu L, Huang G F and Wen S 2017 *Appl. Phys. A* **123** 96
[63] Du M H 2014 *J. Mater. Chem. C* **2** 2475
[64] Yang Z Y, Rudowicz C and Qin J 2002 *Phys. B* **318** 188
[65] Wu S Y, Wei W H and Dong H N 2003 *Z. Naturforsch. A* **58** 672
[66] Tanabe Y and Sugano S 1954 *J. Phys. Soc. Jpn.* **9** 766
[67] Arai T and Adachi S 2011 *J. Appl. Phys.* **110** 063514
[68] Wang Z, Zhou Y, Yang Z, Liu Y, Yang H and Tan H 2015 *Opt. Mater.* **49** 235
[69] Popov D Y, Kavun V Y, Gerasimenko A V, Sergienko V I and Antokhina T F 2002 *J. Coord. Chem.* **28** 19
[70] Hasan Z and Manson N B 1980 *J. Phys. C: Solid State Phys.* **13** 2325
[71] Zhou Q, Zhou Y, Liu Y, Wang Z, Chen G, Peng J, Yan J and Wu M 2015 *J. Mater. Chem. C* **3** 9615